Predicted Film Cooling Near Flush Slots—Comparison with Experiment

D. E. METZGER,* J. H. CARPER JR.,† AND J. M. WARREN‡
Arizona State University, Tempe, Ariz.

The suitability of a finite difference scheme based on parabolic boundary-layer equations for predicting film cooling flows and heat-transfer downstream of flush, angled injection slots is explored. The angled configuration of the slot, which is typical of those employed to cool aerodynamic surfaces on gas turbine engine components, makes flow separation highly probable with the implication that the proper equations describing the flow are elliptic, rather than parabolic. Nevertheless, economy of computation time and compatability with upstream computational methods make retention of the parabolic model desirable if acceptable accuracy is attainable with it. The present study involves measurement of velocity and temperature profiles both upstream and downstream of the injection slot together with heat-transfer rates on the downstream surface. The measured profiles immediately downstream of the slot are used as starting values for prediction of the downstream fields with a parabolic finite difference model similar to that given by Patankar and Spalding. It is found that in the present case of shallow (20°) injection angles, both the downstream fields and surface heat-transfer rates are predicted with acceptable accuracy.

Nomenclature

A = heat-transfer area
c_p = specific heat
G = mass flow rate per unit area
h = heat-transfer coefficient
i = stagnation enthalpy
k = mixing length constant
l = Prandtl mixing length
p = pressure
$\dot{q}$ = heat-transfer rate
s = slot width
t = temperature
u = velocity component in the x-direction
u_τ = shear velocity
V_m = primary freestream velocity
v = velocity component in the y-direction
x = downstream coordinate
y = coordinate normal to surface
y_l = boundary-layer characteristic thickness
β = slot injection angle

δ_D = displacement thickness = $\int_0^\infty \left(1 - \frac{\rho u}{\rho_m V_m}\right) dy$

δ_M = momentum thickness = $\int_0^\infty \frac{\rho u}{\rho_m V_m}\left(1 - \frac{u}{V_m}\right) dy$

λ = mixing length constant
μ_{eff} = effective viscosity
ν = kinematic viscosity
ρ = density
τ = shear stress
ψ = stream function
G^* = mass velocity ratio = G_f/G_m
H = shape factor = δ_D/δ_M
R_M = momentum thickness Reynolds number = $V_m\delta_M/\nu$
St = Stanton number = $h/(G_m c_p)$
u^+ = dimensionless velocity = u/u_τ
y^+ = dimensionless distance yu_τ/ν
θ^* = temperature difference ratio = $(t_f - t_m)/(t_w - t_m)$

Subscripts
av = average over heat-transfer surface
f = film flow, identifies quantities evaluated at the injection slot
m = main flow, identifies quantities evaluated in the freestream
w = wall, identifies quantities evaluated at the surface

Presented as Paper 72-291 at the AIAA 7th Thermophysics Conference, San Antonio, Texas, April 10–12, 1972; submitted May 19, 1972; revision received August 28, 1972.

Index categories: Aircraft Powerplant Design and Installation; Subsonic and Supersonic Airbreathing Propulsion; Boundary Layers and Convective Heat Transfer—Turbulent.

* Professor of Mechanical Engineering. Member AIAA.

† Graduate Student; presently, Senior Engineer, Southwest Research Institute, San Antonio, Texas.

‡ Graduate Student; presently, Major, USAF, Air Force Weapons Laboratory, Kirtland Air Force Base, N. Mex.

Introduction

THE prediction of film-cooling performance has significance in many areas of present day technology, especially in the cooling of high-temperature gas turbine components. Consequently, a very large effort has been expended mainly during the last decade in compiling film-cooling effectiveness for a variety of injection configurations. The majority of this work has been experimental; analysis in general has been satisfactory only far downstream of the injection location, even for two-dimensional situations.

In recent years, as more practical injection configurations are tested in greater detail, it has become evident that conventional correlations of experimental data continue to leave much to be desired. The number of influential variables in any practical situation, indeed in most laboratory experiments, is simply so great as to preclude testing of sufficient combinations to insure confident extrapolation of the separate results. Moreover, empirical correlations are not very compatible with the finite difference methods coming into common use for prediction of velocity and temperature fields on the solid surfaces upstream of injection.

For injection configurations producing downstream flowfields which are essentially two-dimensional, present numerical techniques and machine capabilities offer a definite possibility of extending the finite difference predictions downstream of the injection location. To test this possibility, laboratory experiments are needed, not to provide extensive empirical correlations, but to provide detailed measurements with which to check the accuracy of the particular numerical model. Recently, this type of approach has been used with both parabolic and elliptic models by Pai and Whitelaw[1] and Kacker and Whitelaw[2] for the flowfield downstream of a tangential injection slot with a lip of finite thickness. This injection configuration is shown in Fig. 1a and is representative of slots employed in gas turbine combustor cooling. The presence of separated flow regimes behind the slot lip implies

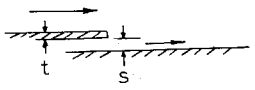

Fig. 1a Tangential injection with finite lip thickness.

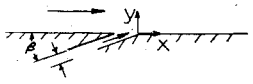

Fig. 1b Flush angled injection.

that the proper differential equations characterizing the downstream flow are elliptic; however, the extent of the separated region and the degree of approximation afforded by a parabolic model are important questions.

The present study treats the flush, angled, two-dimensional injection slot depicted in Fig. 1b. This type of injection configuration is more representative of slots employed on cooled vanes and blades, where aerodynamic considerations dictate the flush opening. Previous work on this particular geometry has been reported by Metzger, et al.[3-5] For this configuration, the film-cooling performance is sensitive to the upstream velocity and temperature profiles, and flow separation downstream of the sharp corner at $x = 0$ again implies that the proper equations are elliptic. The present work involves the careful measurement of velocity and temperature profiles both upstream and downstream of injection, and the corresponding prediction of the downstream fields with a parabolic finite difference scheme similar to the one described by Patankar and Spalding.[6]

Numerical Model

The essential features of the present numerical procedure have been adequately presented by both Patankar and Spalding[6] and subsequent users of the method. Therefore, only the pertinent features of the differential equations, the turbulent transport assumptions, and the solution procedure will be outlined here.

For two-dimensional, steady, boundary-layer flow, the governing continuity, momentum, and energy equations can be written in the following form

$$\partial(\rho u)/\partial x + \partial(\rho v)/\partial y = 0 \tag{1}$$

$$\rho u\, \partial u/\partial x + \rho v\, \partial u/\partial y + dp/dx - \partial\tau/\partial y = 0 \tag{2}$$

$$(\partial/\partial x)(\rho u i) + (\partial/\partial y)(\rho v i) + (\partial/\partial y)(\dot{q}) - (\partial/\partial y)(\tau u) = 0 \tag{3}$$

Introducing the stream function, defined by

$$\rho u = \partial\psi/\partial y \quad \text{and} \quad \rho v = -(\partial\psi/\partial x) \tag{4}$$

Equations (2) and (3) can be transformed to

$$\partial u/\partial x = (\partial\tau/\partial\psi) - (1/\rho u)(dp/dx) \tag{5}$$

$$\partial i/\partial x = -(\partial/\partial\psi)(\dot{q} - u\tau) \tag{6}$$

Equations (5) and (6) are solved numerically with the aid of a mixing length hypothesis for the effective viscosity, μ_{eff}, where

$$\tau = \mu_{\text{eff}}(\partial u/\partial y) \tag{7}$$

The mixing length hypothesis, except for the region near the solid boundary, takes the form

$$\mu_{\text{eff}} = \rho l^2 \left|\frac{\partial u}{\partial y}\right| \tag{8}$$

Based on experimental data collected by Escudier[7] the following variation of the mixing length l is assumed.

$$l = ky \qquad 0 < y < \lambda y_l/k \tag{9}$$

$$l = \lambda y_l \qquad y > \lambda y_l/k \tag{10}$$

Where λ and k are constants, and y_l is a characteristic length equal to the distance from the solid boundary to a point where the velocity differs from the freestream velocity by 1% of the maximum velocity difference across the layer. Near a solid boundary, a modified form of the van Driest[8] hypothesis is used. For a variety of single-fluid, two-dimensional boundary-layer flows, Patankar and Spalding[9] have demonstrated accurate predictions with values of k and λ equal to 0.435 and 0.09, respectively, along with a uniform value of effective Prandtl number equal to 0.9. Carper, [16] in work preliminary to the present study, used these same values to achieve good prediction of the velocity and temperature fields corresponding to the detailed experiments of Hartnett, et al.[11] for film injection through a tangential, nonseparating slot configuration.

It should be noted that these values for k, λ, and effective Prandtl number are based primarily on observations of flows without secondary injection; and, in particular, for flows without the velocity maxima that can accompany injection. It is generally accepted that velocity profile maxima are not predicted well with mixing length theory. Kacker et al.,[12] however, determined that for tangential injection in the manner of Fig. 1a, values of k and λ of 0.435 and 0.09, although not entirely satisfactory, provided the best over all predictions. In the same investigation, they conclude that a linear distribution of effective Prandtl number from 1.75 at the wall to 0.5 in the freestream results in improved predictions over a uniform value. This conclusion was shown by Pai and Whitelaw[1] to be premature, however, and in the present work a uniform value of 0.9 is retained.

The solution procedure employed is basically an implicit marching procedure in which computations proceed downstream following specification of the field variables at some upstream location. In the present case the initial specification is made at $x = 0$ as shown in Fig. 1b from measurements of the mean velocity and temperature profiles obtained from the experimental phase of the investigation.

In the original scheme of Patankar and Spalding,[6] good computational efficiency is achieved by relating the downstream step size to the entrainment rate at the outer edge of the layer. This rule is related in turn to the normal behavior of a single fluid boundary-layer and has proven inappropriate in the present case. For all the results presented in this paper, the size of the downstream step has been controlled independently of the entrainment rate in the region immediately downstream of injection. The details of this stepping procedure are given by Warren.[13]

Experimental Model

The experimental results were obtained in an open cycle wind tunnel with test section dimensions of 16 by 6 in., specifically designed for large scale film injection studies. The primary airflow is induced with a downstream blower capable of providing a test section velocity of 160 fps. The inlet section has a 9 : 1 area contraction ratio designed with methods of Rouse and Hassan.[14] The secondary air is supplied with a separate blower and is metered with a standard orifice. The mainstream flow rates are determined from traverses with a DISA constant temperature hot-wire anemometer system.

The anemometer system is also used to obtain velocity and temperature profiles both upstream and downstream of the injection slot. An indexing controller and stepping motor are used to drive the probe traversing mechanism. The probe position is initially determined optically and the uncertainty in the wire location with respect to the test surface is believed to be less than 0.001 in.

Calibration of the linearized hot wire for velocity measurements is against a Pitot tube in the center of the tunnel test section and is repeatedly checked. The uncertainty in the mean velocity profiles is believed to be less than 1% of the

maximum profile velocity. The anemometer output is measured with an integrating digital voltmeter and recorded on a digital recorder.

For temperature profile measurements the same probe and data acquisition system are used, except the anemometer is operated in a constant current mode. In this mode the output of the anemometer for temperature measurements is linear without the use of a separate linearizer. Calibration of the temperature measurements is accomplished within the tunnel test section. The injected film heated to a temperature of approximately 120°F provides one reference point. The mainstream flow at approximately 74°F is used as the second point. Both air stream temperatures are determined with calibrated copper-constantan thermo-couples used with a self-balancing potentiometric recorder. The uncertainty of the hot wire for temperature measurement is believed to be less than ±0.5°F.

The floor of the tunnel has a length of 58 in. between the end of the inlet contraction section and the flush injection slot. An 18-in. section of 3½ grit sand paper is located on the tunnel floor 38 in. upstream of the slot. The entire downstream section of the tunnel floor, including the downstream side of the slot and the test surface, is mounted on a micrometer traversing mechanism, making the slot width continuously adjustable. The film flow is supplied to the plenum chamber below the slot through electric heaters; screens and foam rubber within the plenum limit spanwise variations in slot velocity to less than 3%. The slot spans the entire 16-in. width of the tunnel floor.

The test surface is installed immediately downstream of the slot, as shown schematically in Fig. 2. The test surface is an aluminum block with 1 in. depth, 6 in. span, and 7 in. length in the downstream direction. The surface heat-transfer rate is determined by establishing the film and mainstream flows at predetermined steady values of velocity and temperature while heating the aluminum block to a temperature in excess of the desired maximum test value. Heating is stopped, and the transient cooling of the block is recorded. The block has negligible internal thermal resistance in comparison with the convective thermal resistance on the upper, or test, surface. This establishes a spatially uniform temperature distribution throughout the block at all times during the cooling transient. The heat-transfer rate on the test surface, with the uniform surface temperature boundary condition, is evaluated by equating the rate of heat loss through the block surfaces to the loss in internal energy of the lumped block thermal capacity. When this is done at different times during the transient for fixed values of the film and mainstream temperatures, t_f and t_m, the heat-transfer rate can be presented as a function of the test surface temperature t_w. Figure 3 shows results of a typical test presented non-dimensionally as St vs θ^* where

$$St = h/(G_m c_p) \tag{11}$$

$$h = (\dot{q}/A)_{av}/(t_w - t_m) \tag{12}$$

$$\theta^* = (t_f - t_m)/(t_w - t_m) \tag{13}$$

In order that the average test surface heat flux, $(\dot{q}/A)_{av}$, be accurately evaluated from the test block transient, the undesired heat leak from the remaining block surfaces must be accounted for. Additional details of this accounting and other aspects of the experimental apparatus and procedure are described by Warren.[13]

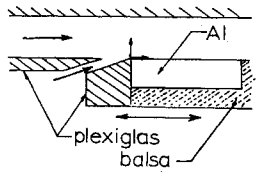

Fig. 2 Schematic of slot and test surface installation.

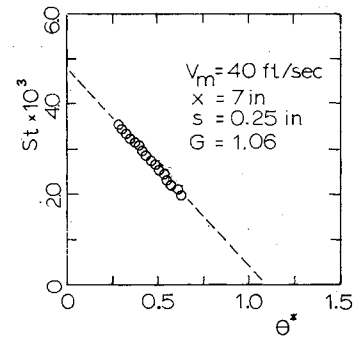

Fig. 3 Typical heat-transfer results.

The use of a film-heating $t_f > t_m$ experiment to model a film-cooling $t_m > t_f$ situation is consistent with an assumption of small temperature differences, negligible property variations, and a corresponding linear governing energy equation. In all the test cases reported in the present study, the temperature differences used were small enough for this assumption to be valid, and the linearity of the results on the graph of Fig. 3 is a direct consequence.

The value of St at $\theta^* = 0$ can be obtained by extrapolation of the linear results of the transient test shown or by conducting a separate transient test with the film temperature equal to the mainstream temperature. In all cases where both methods have been used for identical conditions, the two values of St are identical within the estimated experimental uncertainty of ±8%. To further verify the validity of this transient evaluation procedure, comparative steady-state tests have been conducted and reported.[3] The two sets of results are in excellent agreement.

The value of θ^* at $St = 0$ can similarly be obtained by extrapolation. At this point the surface temperature can be interpreted as an adiabatic value corresponding to zero average surface heat flux. The inverse of θ^* at $St = 0$ for given conditions is a measure, similar to conventional effectiveness, of the mixing between the primary and secondary flows.

Results and Discussion

Upstream Boundary-Layer Development

Exploration of the state of the upstream flow development is important for several reasons in the present investigation. First, the experimental facility was designed to yield predictable, well-behaved growth of the turbulent boundary layer upstream of the injection location. Thus, verification of this growth provides qualification of the instrumentation and data reduction procedures employed. Second, with the flush, angled injection used, the sharp upstream edge of the slot does not produce any appreciable separated flow zone between the primary and secondary streams, in contrast to injection configurations such as shown in Fig. 1a. Thus the character of the upstream velocity and temperature profiles can have a significant effect on the downstream film-cooling performance. Finally, the observed relations between the upstream profiles and the profiles at $x = 0$ can provide guidance for the construction of appropriate starting values for the numerical computations in applications where measured profiles are not available.

Figure 4 shows mean upstream velocity profiles for mainstream velocities of 40, 80, and 120 fps obtained at a location seven slot widths upstream. The velocity is normalized with the freestream velocity V_M and the position of y is normalized with the momentum thickness δ_M. The momentum thickness was obtained from the experimental mean velocity profile by integration. Also shown on Fig. 4 for comparison is a $\frac{1}{7}$ power profile.

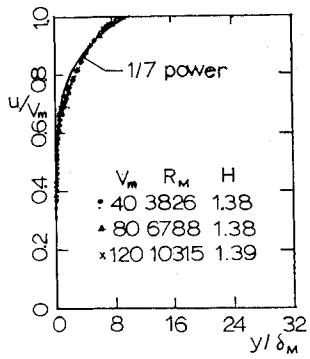

Fig. 4 Measured upstream velocity profiles.

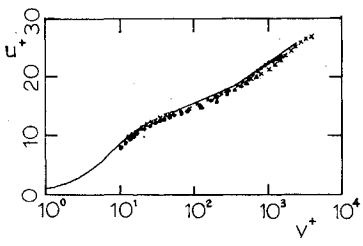

Fig. 5 Measured upstream u^+, y^+ profiles.

Figure 5 shows the same mean velocity profiles on a u^+, y^+ basis where

$$u^+ = u/u_\tau \tag{14}$$

$$y^+ = yu_\tau/\nu \tag{15}$$

$$u_\tau = (g_c\tau_w/\rho)^{1/2} \tag{16}$$

The shear velocity u_τ is evaluated with wall shear stress calculated from the profile momentum thickness by

$$g_c\tau_w/\rho V_m^2 = 0.0125/[V_m\delta_M/\nu]^{1/4} \tag{17}$$

For the profiles on Figs. 4 and 5, the Reynolds number based on momentum thickness, R_M, and the shape factor, H, are shown on Fig. 4. On Fig. 5, the solid line is the four-layer expression given by Reynolds, et al.[15] The smallest y^+ values shown correspond to a distance of about 0.005 in. from the wall. At this spacing correction in the hot wire results because of proximity to the wall[16] was found to be negligible.

Downstream Flow Separation

With the abrupt change in surface direction at $x = 0$, the possibility of a significant separated flow region downstream exists. However, in the present investigation, flow visualization studies using both smoke injection and schlieren photography were carried out. These both indicate that the secondary flow, for an injection angle of 20°, is very effectively turned at $x = 0$, even in the absence of the primary flow. In fact, both the smoke and schlieren visualization fail to indicate any separated region. The hot-wire velocity measurements do, however, indicate that a small region of separated flow is present.

The orientation of the velocity vector at various y positions was determined from measurements with a single wire at two orientations, and was found to vary from 8° at $y = 0.020$ in to 1° at $y = 1.00$ in., for a slot width s of 0.5 in. Figure 6 shows velocities obtained near the wall at various downstream positions between $x = 0$ and $x = 1.0$ in., for $s = 0.25$ in., $V_m = 80$ fps, and $G^* = 0.67$. Linear extrapolations from the closest measured points to zero velocity values at the wall are shown as solid lines. These appear to indicate a thin region of separated flow with length of the order of one slot width downstream.

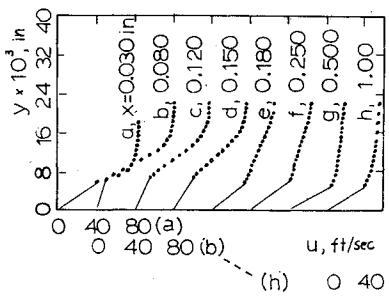

Fig. 6 Measured downstream velocities near injection $s = 0.250$ in., $V_m = 80$ fps, $G^* = 0.67$.

Although no extensive velocity measurements have been made for injection angles other than 20°, flow visualization for an injection angle of 60° does indicate an extensive separated region for injection rates G^* greater than 0.5.

Downstream Measured Velocity and Temperature Fields

In the present study, velocity, temperature, and surface heat-transfer measurements and predictions have been obtained for 20° injections into a uniform velocity mainstream for injection rates over the range $0.6 \leq G^* \leq 1.06$, with slot widths of 0.125, 0.250, and 0.500 in., and nominal mainstream velocities of 40, 80, and 120 fps. In the remaining sections of the paper attention will be focused on three typical sets of conditions and results: $s = 0.250$ in., $V_m = 40.0$ fps, $G^* = 1.06$; $s = 0.250$ in., $V_m = 83.5$ fps, $G^* = 0.67$; and $s = 0.125$ in., $V_m = 120.0$ fps, $G^* = 0.71$.

Figures 7 and 8 show measured velocity and temperature profiles, respectively, for the $G^* = 1.06$ case. For the temperature measurements, the surface temperature was maintained at a steady, uniform value of 116.0°F with film and mainstream temperatures of 118.5°F and 76.6°F, respectively. Figures 9 and 10 show similar profiles for the

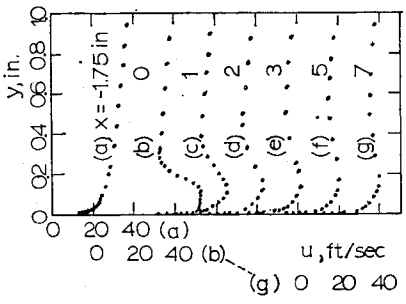

Fig. 7 Measured downstream velocities $s = 0.250$ in., $V_m = 40$ fps, $G^* = 1.06$.

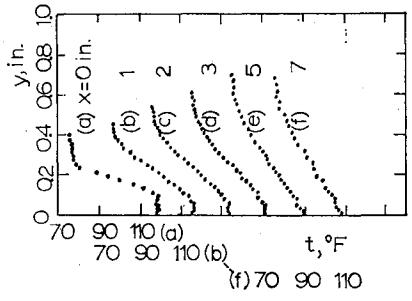

Fig. 8 Measured downstream temperatures $s = 0.250$ in., $V_m = 40$ fps, $G^* = 1.06$.

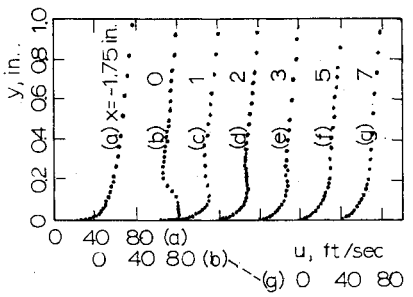

Fig. 9 Measured downstream velocities $s = 0.250$ in., $V_m = 83.5$ fps, $G^* = 0.67$.

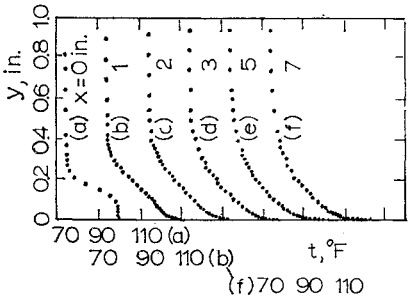

Fig. 10 Measured downstream temperatures $s = 0.250$ in., $V_m = 83.5$ fps, $G^* = 0.67$.

$G^* = 0.67$ case with $t_w = 137.8°F$, $t_f = 100.3°F$, $t_m = 74.2°F$. Figures 11 and 12 present the $G^* = 0.71$ case with $t_w = 128.0°F$, $t_f = 102.8°F$, and $t_m = 74.5°F$. Inspection of the velocity profiles at $x = 0$ shows that the film flow is accelerated and depressed as it turns onto the test surface, and this depression is more noticeable at the lower injection rates. The temperature profiles indicate that good upstream isolation of the film from the heated downstream surface as achieved in the experiments, although it should be emphasized that this will not in general be true in the case of a prototype application.

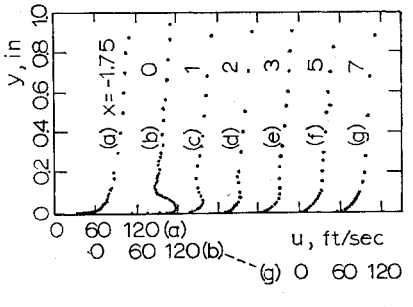

Fig. 11 Measured downstream velocities $s = 0.125$ in., $V_m = 120$ fps, $G^* = 0.71$.

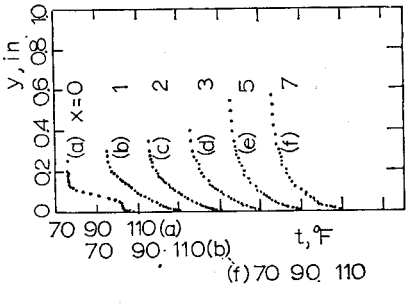

Fig. 12 Measured downstream temperatures $s = 0.125$ in., $V_m = 120$ fps, $G^* = 0.71$.

Comparison with Predicted Downstream Fields

Numerical predictions were obtained using the measured profiles at $x = 0$ as starting values. Differences between the downstream predicted and measured values might be expected to have three causes. First, the measured initial values at $x = 0$ ignore the small, but finite, angle of the velocity vector with respect to the test surface; thus, the initial values used for the numerical computations do not precisely specify the fields at that point. Second, the numerical computations assume that the situation is governed by the parabolic boundary-layer equations. This again is not precisely correct. Third, the assumed turbulent transport laws may be inadequate for this flow situation, especially with the presence of local velocity maxima.

Figure 13 shows a typical set of predicted and measured velocity and temperature profiles for conditions corresponding to those of Figs. 9 and 10, for $k = 0.435$, $\lambda = 0.09$, and effective Prandtl number uniform at a value of 0.9. The predicted profiles are indicated by the solid lines. In general the agreement is quite good, except for the overpredicted velocities in the region near the wall. It might be speculated that the mixing lengths used in this region do not provide sufficient mixing of the injected film with the mainstream; however, experimental mixing lengths obtained by Warren[13] do not support this conclusion.

This is somewhat substantiated by the results shown in Fig. 14, where the same situation was predicted with the identical mixing length and effective Prandtl number assumptions, but where the starting profiles are the measured values obtained at $x/s = 4.0$. At this point downstream, any separated flow should have reattached, and the boundary-layer equations should represent the flow adequately. As can be seen in Fig. 14, the predictions, especially of the velocity profiles, are improved over those of Fig. 13.

Figure 15 presents results for the same situation, with measured profiles at $x = 0$ used as starting values, but with an effective Prandtl number distribution varying linearly from a value of 1.5 at the wall to a value of 0.5 in the freestream.

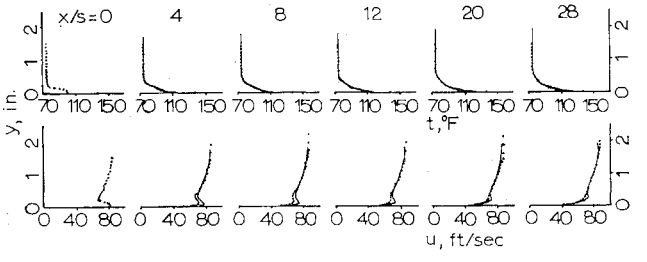

Fig. 13 Comparison of predicted and measured downstream velocity and temperature $s - 0.250$ in., $V_m - 83.5$ fps, $G^* - 0.67$, $k - 0.435$, $\lambda - 0.09$ uniform effective Prandtl no., starting values measured at $x - 0$.

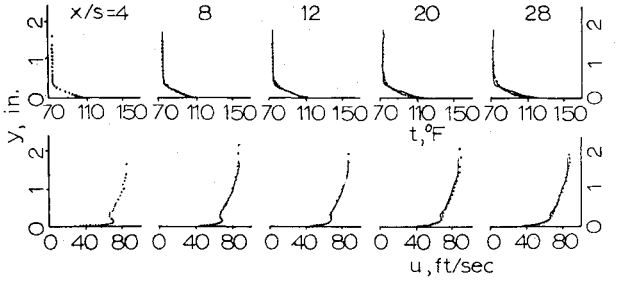

Fig. 14 Comparison of predicted and measured downstream velocity and temperature $s - 0.250$ in., $V_m - 83.5$ fps, $G^* - 0.67$, $k - 0.435$, $\lambda - 0.09$ uniform effective Prandtl no., starting values measured at $x - 1.0$ in.

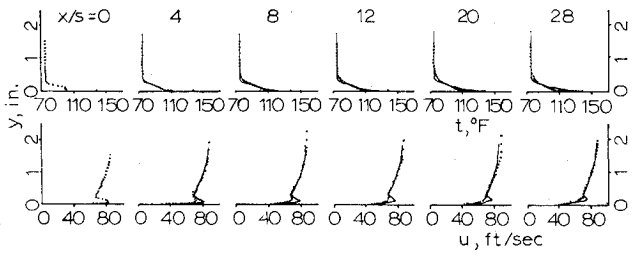

Fig. 15 Comparison of predicted and measured downstream velocity and temperature $s - 0.0250$ in., $V_m - 83.5$ fps, $G^* - 0.67$, $k - 0.435$, $\lambda - 0.09$ linear effective Prandtl no. distribution, starting values measured at $x - 0$.

In comparison to the corresponding results with a uniform distribution, the predictions do not appear to be very sensitive to this magnitude of change in effective Prandtl number.

Comparison of Measured and Predicted Heat Transfer

Figures 16–18 summarize the measured and predicted average surface heat transfer over the 7 in. test surface for the $G^* = 1.06$, 0.67, and 0.71 cases, respectively. The solid line in Fig. 16 is a least-square fit through the data points shown in Fig. 3. Likewise, the solid lines in Fig. 17 and 18 represent best-fit straight lines through the corresponding experimentally determined Stanton numbers. The numerically predicted heat-transfer rates, averaged over a downstream length of 7 in., are indicated by symbols at various values of θ^*. The predictions for θ^* values different than those shown in Figs. 8, 10, and 12 were obtained by modifying the measured temperature profiles at $x = 0$ in the region very close to the wall such that the profile fairs smoothly to the surface temperature yielding the desired value of θ^*. These modified temperature profiles, together with the velocity profiles, were then used as starting profiles for the numerical computations.

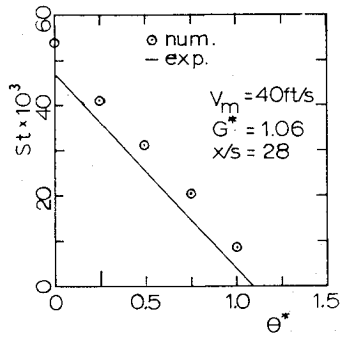

Fig. 16 Predicted and measured *St*.

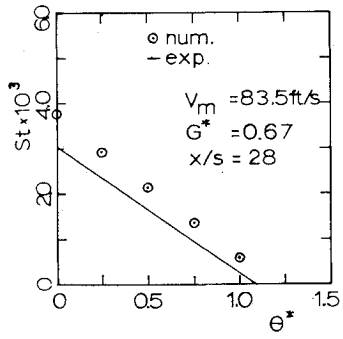

Fig. 17 Predicted and measured *St*.

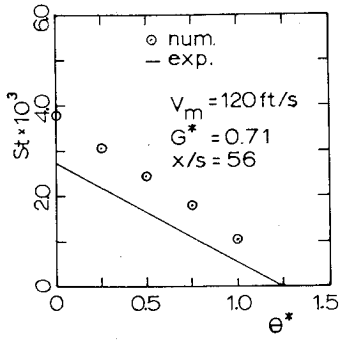

Fig. 18 Predicted and measured *St*.

If a best-fit straight line is passed through the predicted Stanton numbers than the predicted intercept at $\theta^* = 0$ ranges from 15% to 38% higher than the measured values. If the inverse of the intercept when $St = 0$ is intrepreted as film-cooling effectiveness, then the predicted average effectiveness is approximately 8% low in all three cases.

Thus the mixing between the primary and secondary streams, which governs the effectiveness, appears to be quite accurately predicted with the present model, although the temperature gradient at the wall, and thus the heat-transfer rate, is predicted significantly less accurately. However, it should be noted that most film-cooling predictions for design purposes are done with correlations of effectiveness only, and the heat-transfer coefficient used is that associated with the primary flow alone. Also, the largest variations in measured effectiveness, even for apparently similar injection configurations, occur in the range of effectivenesses covered in the present study. Consequently, even a difference of 38% in predicted and actual heat-transfer rates is not much worse than might be expected using conventional effectiveness correlations.

Conclusions

The principal conclusions of the present study can be summarized as follows: 1) With secondary injection through flush, angled, two-dimensional injection slots, flow separation is observed downstream of the sharp rear edge of the slot. The extent and influence of the separated region, however, appear to be small for injection at 20° with mass-velocity ratios up to unity. For smaller injection angles and/or rounding of the slot rear edge, the separated flow region is likely to be even smaller. 2) Reasonably good prediction of the downstream temperature and velocity fields can be made numerically with parabolic boundary-layer equations and a standard mixing length model for the turbulent transport mechanism. The predicted profiles should be adequate for use in assessing the effects of changes in injection parameters on the outer flow for a variety of practical, film-cooled components. 3) The average surface heat-transfer rates in the important region immediately downstream of the injection slot can also be predicted in similar fashion to a degree of accuracy that is acceptable for many engineering applications. The important implication is that a relatively straight-forward, economical numerical technique can be employed to explore the effects of a wide range of influential film-cooling variables such as upstream profile perturbations in the main and/or the film streams, and property variations related to large temperature differences between the two flows and between the flows and the solid surface.

References

[1] Pai, B. R. and Whitelaw, J. H., "The Prediction of Wall Temperature in the Presence of Film Cooling," *International Journal of Heat and Mass Transfer*, Vol. 14, 1971, pp. 409–426.

[2] Kacker, S. C. and Whitelaw, J. H., "Prediction of Wall-Jet and Wall-Wake Flows," *Journal of Mechanical Engineering Science*, Vol. 12, No. 6, 1970, pp. 404–420.

[3] Metzger, D. E., Carper, H. J., and Swank, L. R., "Heat Transfer with Film Cooling Near Non-Tangential Injection Slots," *Transactions of the ASME: Journal of Engineering for Power; Ser. A*, Vol. 90, 1968, pp. 157–163.

[4] Metzger, D. E. and Fletcher, D. C., "Evaluation of Heat Transfer for Film-Cooled Turbine Components," *Journal of Aircraft*, Vol. 8, No. 1, Jan. 1971, pp. 33–38.

[5] Metzger, D. E., Biddle, J. R., and Warren, J. M., "Evaluation of Film Cooling Performance on Gas Turbine Surfaces," *High Temperature Turbines*, AGARD Publication CP-73-7, 1971.

[6] Patankar, S. V. and Spalding, D. B., "A Finite-Difference Procedure for Solving the Equations of the Two-Dimensional Boundary Layer," *International Journal of Heat and Mass Transfer*, Vol. 10, 1967, pp. 1389–1411.

[7] Escudier, M. P., "The Distribution of Mixing Length in Turbulent Flows Near Walls," Mechanical Engineering Rept. TWF/TN/1, 1965, Imperial College, London, England.

[8] van Driest, E. R., "On Turbulent Flow Near a Wall," *Journal of the Aeronautical Sciences*, Vol. 23, 1956, p. 1007.

[9] Patankar, S. V. and Spalding, D. B., *Heat and Mass Transfer in Boundary Layers*, Morgan-Grampian Press, London, England, 1967.

[10] Carper, H. J., "Velocity Distributions and Heat Transfer with Film Cooling Near a Single, Angled, Spanwise-Continuous Slot: A Numerical and Experimental Study," Ph.D. dissertation, 1969, Arizona State Univ. Tempe, Ariz.

[11] Hartnett, J. P., Birkebak, R. C., and Eckert, E. R. G., "Velocity Distributions, Effectiveness, and Heat Transfer for Air Injected Through a Tangential Slot into a Turbulent Boundary Layer," *Transactions of the ASME: Journal of Heat Transfer; Ser. C*, Vol. 83, 1961, pp. 293–306.

[12] Kacker, S. C., Pai, B. R., and Whitelaw, J. H., "The Prediction of Wall-Jet Flows with Particular Reference to Film Cooling," *Progress in Heat and Mass Transfer*, Vol. 2, Pergamon Press, Oxford, 1969, pp. 163–186.

[13] Warren, J. M., "Velocity and Temperature Distributions, Turbulence Characteristics and Heat Transfer with Film Cooling and Variable Freestream Velocity: A Numerica land Experimental Study," Ph.D. dissertation, 1971, Arizona State University, Tempe, Ariz.

[14] Rouse, H. and Hassan, M. M., "Cavitation-Free Inlets and Contractions," *Mechanical Engineering*, Vol. 71, Feb 1949, pp. 213–216.

[15] Reynolds, W. C., Kays, W. M., and Kline, S. J., "Heat Transfer in the Turbulent Incompressible Boundary Layer," Memo. 12-1-58W, 1958, NASA.

[16] Lawn, C. J., "Turbulence Measurements With Hot Wires at B.N.L.," National Bureau of Standards Rept. No. N69-36431, April 1969, U. S. Department of Commerce.